J Mater Sci (2010) 45:2574–2579
DOI 10.1007/s10853-010-4228-7

Hierarchical constraint distribution of ultra-high molecular weight polyethylene fibers with different preparation methods

Masaki Kakiage · Takuya Tamura · Syozo Murakami · Hiroshi Takahashi · Takeshi Yamanobe · Hiroki Uehara

Received: 1 October 2009 / Accepted: 11 January 2010 / Published online: 4 March 2010

Abstract The hierarchical constraint characteristics of ultra-high molecular weight polyethylene (UHMW-PE) fibers with different structures were evaluated by in situ wide-angle X-ray diffraction (WAXD) measurement during heating. Two UHMW-PE fibers were used in this study, an original gel-spun fiber and a processed fiber that was tensile-drawn from the original fiber above the static equilibrium melting temperature of PE. A difference in fiber processing induced change in constraint distribution attributed to morphological heterogeneity. The original gel-spun fiber, which had a heterogeneous structure, induced the constraint distribution because of the obvious existence of skin and core. In contrast, the tensile-drawn fiber, which had a homogeneous structure formed by the fusion adhesion between twisted single yarn surfaces, depressed the constraint distribution. These results demonstrate that a difference in fiber processing induces change in hierarchical characteristics with different structural dimensions.

Masaki Kakiage is a Research Fellow of the Japan Society for the Promotion of Science.

M. Kakiage · T. Tamura · T. Yamanobe · H. Uehara (✉)
Department of Chemistry and Chemical Biology, Gunma University, Kiryu, Gunma 376-8515, Japan
e-mail: uehara@chem-bio.gunma-u.ac.jp

S. Murakami
Heian Jogakuin University, Takatsuki, Osaka 569-1092, Japan

H. Takahashi
Department of Chemistry and Chemical Biology, Biophysics Laboratory, Graduate School of Engineering, Gunma University, 4-2, Aramaki, Maebashi 371-8510, Japan

Present Address:
M. Kakiage
Department of Applied Chemistry, Saitama University, 255 Shimo-Okubo, Sakura-ku, Saitama 338-8570, Japan

Introduction

Polyethylene (PE) fiber is a typical high-performance material that is widely applied in producing rope and textiles. It is produced by the gel-spinning method, which allows a PE chain with ultra-high molecular weight (UHMW) to become highly oriented along the fiber direction [1]. The orientation state greatly influences its performance (e.g., tensile modulus and strength).

When an oriented PE sample was heated under tension, an orthorhombic phase transformed through an intermediate hexagonal phase into melt [2–13]. This hexagonal phase also appeared during drawing from the molten state of UHMW-PE [14–16]. Considering that the crystal modification of the hexagonal phase is the same as that of the extended-chain crystal that is usually formed under high temperature and pressure [17–21], it can be reasonably assumed that this highly oriented chain arrangement significantly affects the phase transition behavior during heating of preoriented PE. Tsubakihara et al. [5] reported on the melting characteristics under fixed conditions of commercial PE fibers with different MWs. The phase transition and melting mechanisms were analyzed based on a free-energy diagram.

However, such a phase transition during heating of the oriented PE sample is also synchronized with its stress relaxation [2, 4, 6]. Moreover, we reported that the morphology of the sample corresponded to retractive stress for melt-drawn UHMW-PEs with different molecular characteristics [13]. Therefore, the stress state inside oriented PE fiber can closely relate to both the obvious orientation state and to the fiber morphology.

In this study, we discussed phase transition behavior during heating of UHMW-PE fibers with different preparation methods in order to define the constraint characteristics of fibers with different structures, using in situ wide-angle X-ray diffraction (WAXD) measurement during heating. One sample is an original gel-spun fiber, and the other is a processed fiber that is tensile-drawn from the original fiber above the static equilibrium melting temperature of PE ($T^0_{m,PE}$). The fiber morphologies with different preparation methods were investigated using scanning electron microscopy (SEM).

Fiber material generally has a "skin" and a "core" in each single yarn, which contribute to the intrinsic heterogeneity inside the fiber structure (e.g., crystalline form or orientation state) and the properties (e.g., wear resistance or processing reactivity to cross-linking). Constraint distribution arises from this structural heterogeneity. The constraint distribution for the material varies, since the skin is more constrained by this process, although the core maintains a state of high constraint after the fusion adhesion process. Furthermore, the entire fiber morphology is modified by this process (i.e., more homogeneous morphology for the skin-molten PE fiber). Therefore, understanding such hierarchical characteristics is highly important for processing PE fiber material. Thermal analysis using differential scanning calorimetry (DSC) is a common tool for evaluating the fiber structure, because it reasonably responds to crystalline modification or orientation state. However, it is difficult to attribute multiple peaks to the phase transition or melting of crystals because the meaning of a peak is amphibological, depending on the constraint state of the fiber, i.e., tightly fixed [7, 22] or tension-free [22] conditions. In situ WAXD measurement during heating enables us to determine the origin of these crystalline transformations because the phase transition from the orthorhombic phase into the hexagonal phase is in accordance with a stress–temperature phase diagram [13]. Ratner et al. [11] discussed the phase transition behavior in UHMW-PE fiber compacts prepared by different compression conditions with surface cross-linking, based on DSC and in situ WAXD measurements. In this study, the correlation between phase transition behavior and the hierarchical constraint characteristics of UHMW-PE fiber was investigated from diversified perspectives combining morphological and phase transition considerations.

Experimental

Materials

Two UHMW-PE fibers were used in this study, Dyneema (Toyobo Co. Ltd., Japan) and a tensile-drawn fiber (TD-fiber). Dyneema is a typical UHMW-PE strand prepared by the gel-spinning method and has a higher tensile modulus and strength despite being lightweight. The TD-fiber was prepared by tensile-drawing the Dyneema strand at 145 °C, above the $T^0_{m,PE}$, and 30% elongation, which induces fusion adhesion between twisted single yarn surfaces. Before drawing, the sample specimen was held at 145 °C for 5 min for temperature equilibrating with on tension. The crosshead speed of drawing was 24 mm/min. It has been known that a UHMW-PE material could be drawn even from the molten state using its higher melt viscosity [13–16, 23–28].

Measurements

Morphologies of these fiber samples were observed by using a Hitachi field-emission SEM S-4800 operated at 1.0 kV. The sample was non-coated, thus any artifact was negligible. In situ WAXD measurements during the heating process were carried out using a synchrotron radiation source at Beamline 9C of the Photon Factory at the High Energy Accelerator Research Organization (KEK) in Tsukuba, Japan. The wavelength of the synchrotron beam was 1.50 Å. The UHMW-PE fibers were wound tightly on a copper sample holder in a high-temperature furnace installed in the beamline, where the measurement temperature was detected by thermocouples placed less than 1 mm away from the sample. All heating was performed up to sample breaking at a rate of 2 °C/min. WAXD profiles were continuously recorded with a 29 s exposure time for each pattern and a 1 s time interval. A position sensitive proportional counter (PSPC) (Rigaku, PSPC-10), which was used to detect diffraction intensity, was attached along the equatorial direction on the fiber axis.

Results and discussion

SEM observations were carried out in order to characterize the surface morphologies of these UHMW-PE fibers with different preparation methods. Figure 1 presents SEM images of Dyneema and TD-fiber. The diameter of a monofilament is approximately 30 μm. The agglomerates on a micrometer scale, which were formed by melt-recrystallization in the fiber surface during the tensile-drawing process above the $T^0_{m,PE}$, are observed for the TD-fiber (Fig. 1c). In contrast, the location of fiber boundaries is recognized for Dyneema (Fig. 1b), although only flatter morphology is observed for the TD-fiber (Fig. 1d). This means that the fusion adhesion between twisted single yarn surfaces is developed by tensile-drawing process at 145 °C. These results indicate that structural homogeneity of the TD-fiber is higher than that of Dyneema.

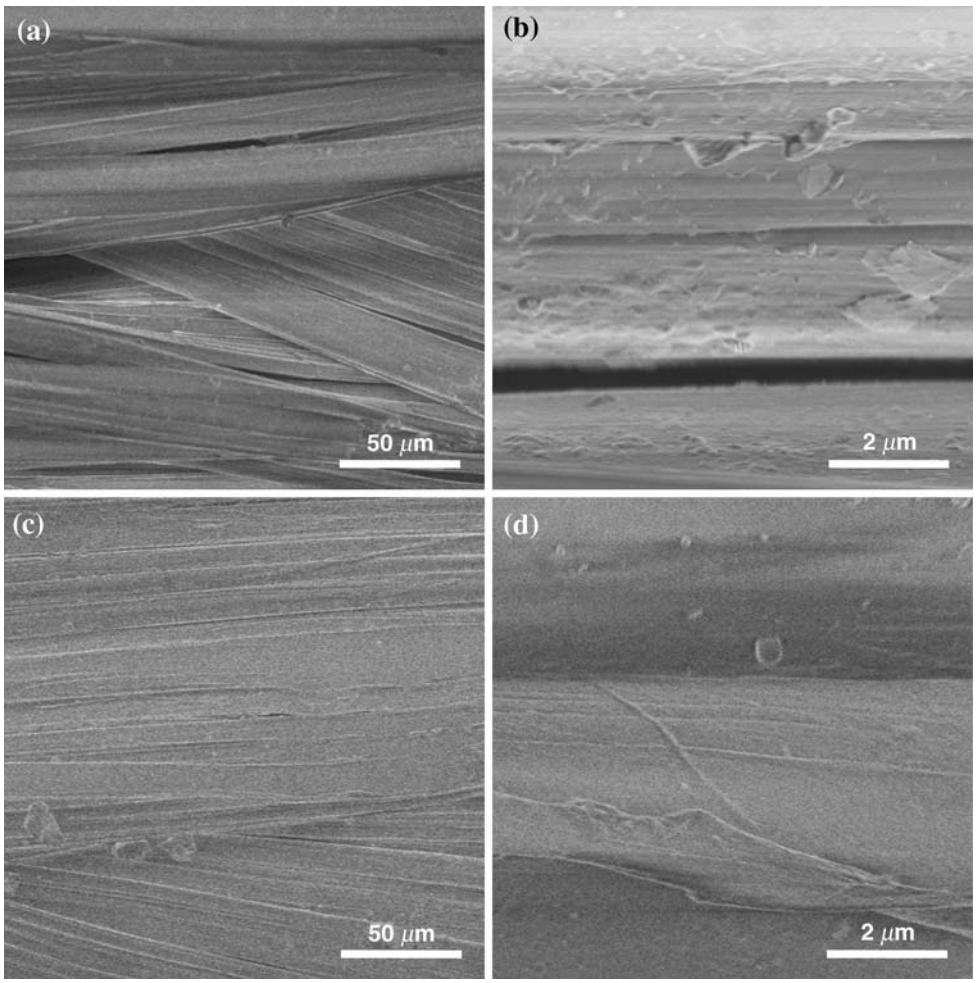

Fig. 1 SEM images of **a**, **b** Dyneema and **c**, **d** TD-fiber

In situ WAXD measurement for both fibers during heating was carried out for qualitative analysis of the structural change. The obtained 2θ profiles are plotted as a function of temperature in Figs. 2 and 3. For Dyneema (Fig. 2), weaker monoclinic (010) reflection is exhibited and disappears at 130 °C, since a small amount of monoclinic crystal is located in the UHMW-PE fiber skin [29]. Additionally, the intensities of orthorhombic (110) and (200) reflections increase gradually for Dyneema, indicating the rearrangement of PE crystals with the thermal treatment. The transition from the orthorhombic phase into the hexagonal phase occurs beyond 145 °C, with no remarkable increase of amorphous scattering (Fig. 2b). However, its phase transition is gentle, and the intensity of hexagonal (100) reflection is consequently weaker. The fiber breaks at 155 °C. In contrast, for the TD-fiber (Fig. 3), no monoclinic (010) reflection is observed because the monoclinic crystal located in the fiber skin disappeared during the tensile-drawing process under higher temperature. Moreover, no significant increase of orthorhombic (110) reflection is observed, due to the annealing effect under high temperature during fiber preparation. Phase transition behavior is more significant than for Dyneema, and only hexagonal (100) reflection is observed beyond 154 °C, with increasing amorphous scattering (Fig. 3b). The fiber breaks at 159 °C, which is 4 °C higher than that for Dyneema.

The differences in phase transitions during the heating of these fibers were characterized using the integral intensities of the crystalline reflections observed by in situ WAXD measurement. The obtained line profiles (Figs. 2 and 3) were resolved into hexagonal (100), and orthorhombic (110) and (200) reflection peaks using the Voigt function, which combines the Lorentzian and Gaussian functions. Here, small amorphous scattering was ignored because quantitative fitting was impossible. Among the resolved peaks, the hexagonal (100) and orthorhombic (110) ones were chosen for evaluation of the crystalline phase transition. Changes in the integral intensities of these peaks during heating of Dyneema and TD-fiber are summarized in Fig. 4. For Dyneema (top column), the transition into the hexagonal phase is recognized from 145 °C but remains incomplete, with the orthorhombic phase surviving. This incomplete transition temperature window with the

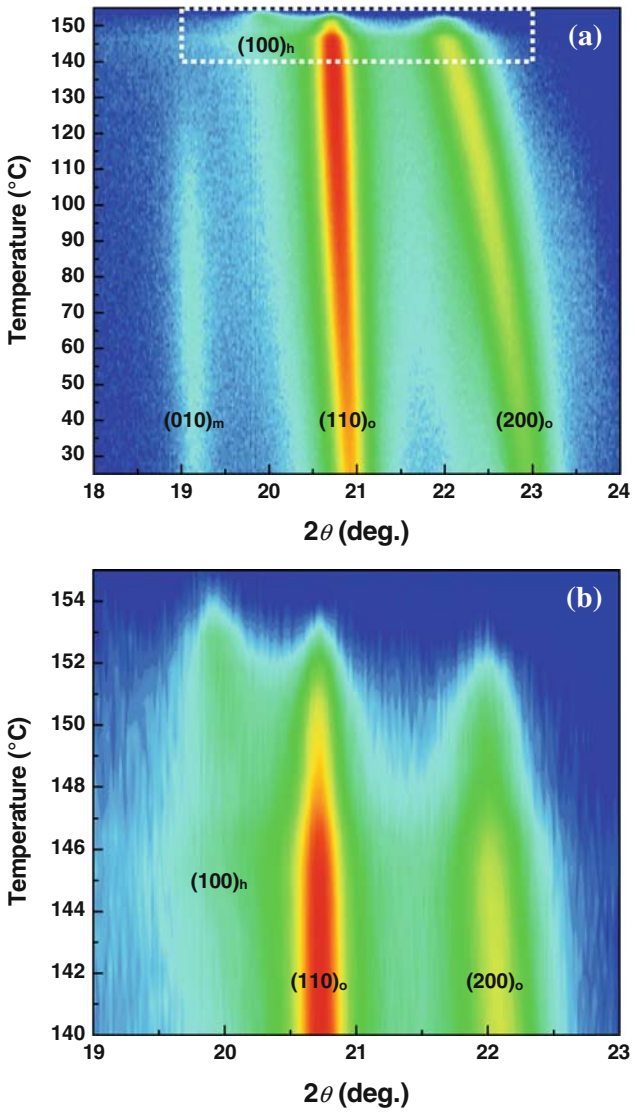

Fig. 2 **a** Changes in WAXD patterns during heating for Dyneema. The difference in intensity is represented by a color gradation with a logarithmic scale indicating intensity from the lowest (*blue*) to the highest (*red*). Subscript "o" corresponds to the orthorhombic phase, "h" to the hexagonal phase, and "m" to the monoclinic phase. **b** Enlarged figure of the area surrounded by the *white dotted square* in **a**. (Color figure online)

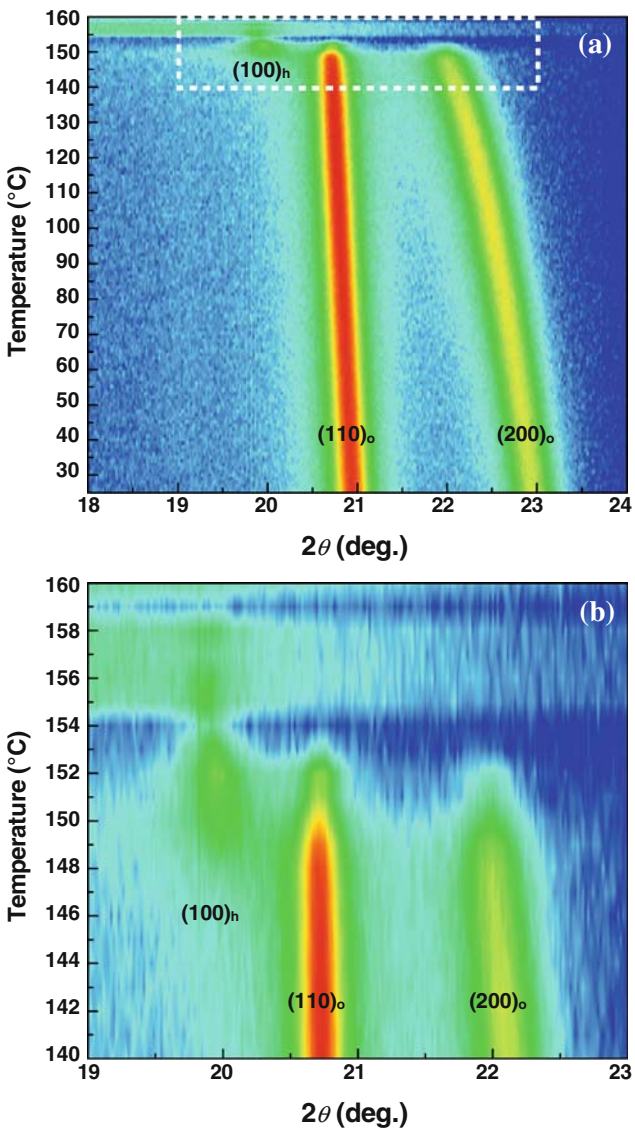

Fig. 3 **a** Changes in WAXD patterns during heating for TD-fiber. **b** Enlarged figure of the area surrounded by the *white dotted square* in **a**

coexistence of the hexagonal and orthorhombic phases reaches 8 °C. Complete transition into the hexagonal phase is recognized at 154 °C, just before the sample breaks at 155 °C. Consequently, the complete transition temperature window with only the hexagonal phase is depressed. The behavior of the incomplete transition temperature window for the TD-fiber (bottom column) is similar to that for Dyneema. However, the complete transition temperature window with only the hexagonal phase reaches 5 °C from 154 °C, which is broader than that for Dyneema.

We reported that such a temperature window observed during heating of the melt-drawn UHMW-PE samples with different molecular characteristics is deeply related to the retractive stress attributed to its morphology [13]. Specifically, the behavior of this temperature window reflected crystalline structural homogeneity on a nanometer scale. A sample with heterogeneous structure exhibited both less perfection of the phase transition and a narrower complete transition temperature window due to the constraint distribution with partial sample retraction. In contrast, a sample with homogeneous structure had a broader complete transition temperature window. This correlation between structural homogeneity and phase transition behavior is also recognized in this study, although only structural homogeneity on a micrometer scale is different (Fig. 1). Namely, Dyneema, which has a heterogeneous structure, exhibits the narrower complete transition temperature window (Fig. 4, top column), and the TD-fiber,

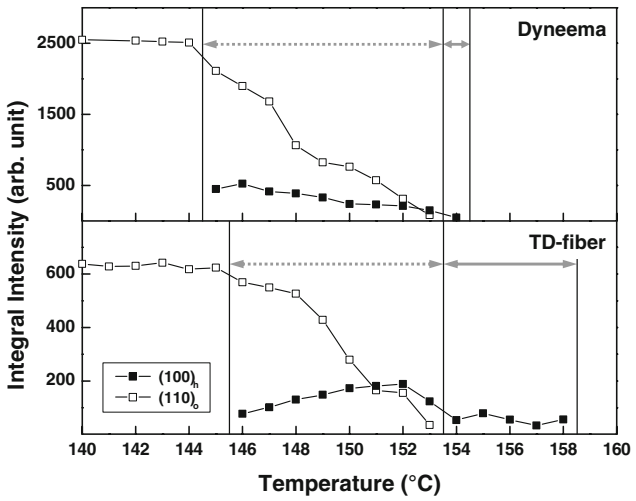

Fig. 4 Changes in the integral intensities of the hexagonal (100) and orthorhombic (110) reflection peaks evaluated from the WAXD profiles in Figs. 2 and 3: (*top*) Dyneema and (*bottom*) TD-fiber. The *broken arrows* indicate the incomplete transition temperature window, and the *solid arrows* indicate the complete transition temperature window

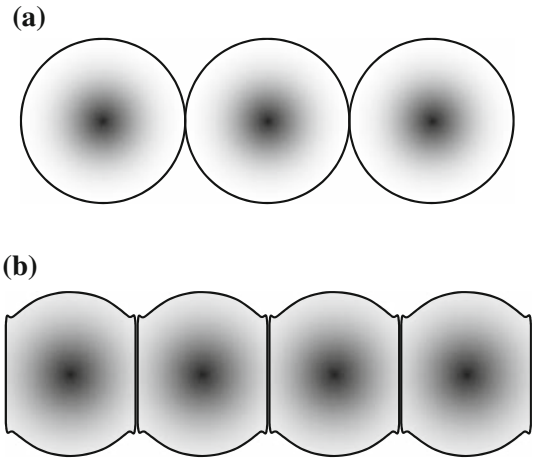

Fig. 5 Schematic interpretations of constraint distribution for **a** Dyneema and **b** TD-fiber. Dyneema is the strand consisting of original single yarns, and the TD-fiber is the cohesive fiber prepared by fusion adhesion between twisted single yarn surfaces. The difference in constraint state is represented by a color gradation indicating a state of less constraint (*bright*) and more constraint (*dark*)

which has a homogeneous structure, exhibits the broader complete transition temperature window (Fig. 4, bottom column). Here, the difference in phase transition behavior for UHMW-PE fiber points to that in constraint state inside fiber because the stress–temperature phase diagram dominates this phase transition behavior [13]. Thus, the homogeneity of structure corresponds to that of constraint state. This knowledge indicates that the TD-fiber with a broader complete transition temperature window has a homogeneous fiber structure, indicating less constraint distribution inside the fiber; in contrast, Dyneema, with a heterogeneous structure, exhibits constraint distribution. Considering the existence of these components with different constraint states, it is assumed that the constraint-free component corresponds to the skin and the constant-constraint component corresponds to the core of a single yarn. These results demonstrate that the difference in constraint states is induced by the preparation methods.

Schematic interpretations of constraint distribution for both fibers are proposed in Fig. 5, based on the experiment result of this in situ WAXD measurement during heating. Essentially, the two fibers used in this study, Dyneema and TD-fiber, consist of the same UHMW-PE single yarns prepared by the gel-spinning method. The skin and core contribute to the intrinsic structural heterogeneity inside the fiber. The skin is in a state of less constraint (bright area in Fig. 5), while the core is in a state of more constraint (dark area in Fig. 5). Here, the tensile-drawing process above the $T^0_{m,PE}$ for the TD-fiber induces sufficient fusion adhesion between the twisted single yarn surfaces. Significant disruption of the balance of intrinsically included skin and core for the single yarn leads to a change in constraint distribution as a result of this tensile-drawing process. For Dyneema (Fig. 5a), an obvious skin exists because the structure of the original single yarn remains after twisting (i.e., the single yarn of Dyneema has a heterogeneous structure). This structural characteristic induces the constraint distribution inside the fiber. In contrast, for the TD-fiber (Fig. 5b), a monostructure is formed by the fusion adhesion between twisted single yarn surfaces during the tensile-drawing process (i.e., the single yarn of TD-fiber has a more homogeneous structure). Consequently, the constraint core area increases, although the skin decreases. Thus, the constraint distribution is depressed and more constraint is achieved for the single yarn of TD-fiber. Therefore, the transition behavior from the orthorhombic phase into the hexagonal phase becomes significant, and the complete transition temperature window existing in only the hexagonal phase is broader because a state of more constraint can be maintained at high temperature. Furthermore, morphological homogeneity across the whole fiber is modified significantly by the tensile-drawing process, which affects the phase transition behavior and the mechanical properties. Indeed, the tensile-drawing process above the $T^0_{m,PE}$ changes the morphology and mechanical properties of a rolled film by direct processing from UHMW-PE reactor powder [30]. For Dyneema (Fig. 5a), the constraint state for each single yarn is different, since a separate single yarn exists inside the fiber (i.e., heterogeneous morphology). Thus, heterogeneity of phase transition behavior is induced because the phase transition proceeds independently for each single yarn under different constraint states. Moreover, the breaking temperature is lower because breaking occurs discretely for each single

yarn, in accordance with the constraint state. In contrast, for the TD-fiber (Fig. 5b), cohesiveness of the original single yarn is achieved by the tensile-drawing process. The obtained homogeneous morphology contributes to the broader complete transition temperature window existing in only the hexagonal phase and the higher breaking temperature, because the core (i.e., the component with more constraint) increases for the cohesive fiber. These results demonstrate that a difference in fiber processing induces change in hierarchical characteristics with different structural dimensions (i.e., constraint distribution of skin and core into a single yarn, and morphological homogeneity across the whole fiber). This structural development for the tensile-drawn fiber acts on the resultant mechanical properties (i.e., improvement of heat and wear resistances of the fiber). Furthermore, the surface and constraint characteristics of initial fibers affect the mechanical properties of PE fiber applications (e.g., a fiber-reinforced composite [31–33] and a compacted material [11, 34, 35]). Therefore, findings from this study provide a methodology for preparing and developing polymeric materials.

Conclusions

The hierarchical constraint characteristics of UHMW-PE fibers with different structures were evaluated by in situ WAXD measurement during heating. Two UHMW-PE fibers were used in this study; Dyneema was the original gel-spun fiber, and the TD-fiber was the processed fiber that was tensile-drawn from the original fiber above the $T^0_{m,PE}$. The obtained result suggested that the difference in constraint distribution is induced by the preparation method. Dyneema, which had a heterogeneous structure, induced the constraint distribution inside the fiber because the obvious skin existed. In contrast, the TD-fiber, which had a homogeneous structure, depressed this constraint distribution because a mono-structure-like core was formed by the fusion adhesion between the single yarn surfaces during the tensile-drawing process. These results demonstrated that significant disruption of the balance of intrinsically included skin and core led to a change in the constraint distribution inside the fiber and morphological homogeneity across the whole fiber as a result of this tensile-drawing process.

Acknowledgements Synchrotron WAXD measurements were performed under the approval of the Photon Factory Program Advisory Committee (Proposal 2004G265). This work was partly supported by a Grant-in-Aid for the Japan Society for the Promotion of Science (JSPS) Fellows and the Industrial Technology Research Grant Program from the New Energy and Industrial Technology Development Organization (NEDO) of Japan. M. Kakiage expresses his gratitude for the JSPS Research Fellowships for Young Scientists.

References

1. Smith P, Lemstra PJ (1980) J Mater Sci 15:505. doi:10.1007/BF00551705
2. Pennings AJ, Zwijnenburg A (1979) J Polym Sci Polym Phys Ed 17:1011
3. Murthy NS, Correale ST, Kavesh S (1990) Polym Commun 31:50
4. Rastogi S, Odell JA (1993) Polymer 34:1523
5. Tsubakihara S, Nakamura A, Yasuniwa M (1996) Polym J 28:489
6. Uehara H, Kanamoto T, Kawaguchi A, Murakami S (1996) Macromolecules 29:1540
7. Tashiro K, Sasaki S, Kobayashi M (1996) Macromolecules 29:7460
8. Kuwabara K, Horii F (1999) Macromolecules 32:5600
9. Kwon YK, Boller A, Pyda M, Wunderlich B (2000) Polymer 41:6237
10. Rein DM, Shavit L, Khalfin RL, Cohen Y, Terry A, Rastogi S (2004) J Polym Sci B Polym Phys 42:53
11. Ratner S, Weinberg A, Wachtel E, Moret PM, Marom G (2004) Macromol Rapid Commun 25:1150
12. Watanabe S, Dybal J, Tashiro K, Ozaki Y (2006) Polymer 47:2010
13. Kakiage M, Sekiya M, Yamanobe T, Komoto T, Sasaki S, Murakami S, Uehara H (2008) J Phys Chem B 112:5311
14. Uehara H, Kakiage M, Yamanobe T, Komoto T, Murakami S (2006) Macromol Rapid Commun 27:966
15. Kakiage M, Yamanobe T, Komoto T, Murakami S, Uehara H (2006) J Polym Sci B Polym Phys 44:2455
16. Kakiage M, Yamanobe T, Komoto T, Murakami S, Uehara H (2006) Polymer 47:8053
17. Wunderlich B, Arakawa T (1964) J Polym Sci A Polym Chem 2:3697
18. Bassett DC, Turner B (1972) Nature (London) Phys Sci 240:146
19. Asahi T (1984) J Polym Sci Polym Phys Ed 22:175
20. Rastogi S, Kurelec L, Lemstra PJ (1998) Macromolecules 31:5022
21. Kurelec L, Rastogi S, Meier RJ, Lemstra PJ (2000) Macromolecules 33:5593
22. Lacroix Fv, Loos J, Schulte K (1999) Polymer 40:843
23. Bashir Z, Keller A (1989) Colloid Polym Sci 267:116
24. Uehara H, Nakae M, Kanamoto T, Zachariades AE, Porter RS (1999) Macromolecules 32:2761
25. Nakae M, Uehara H, Kanamoto T, Ohama T, Porter RS (1999) J Polym Sci B Polym Phys 37:1921
26. Nakae M, Uehara H, Kanamoto T, Zachariades AE, Porter RS (2000) Macromolecules 33:2632
27. Kakiage M, Sekiya M, Yamanobe T, Komoto T, Sasaki S, Murakami S, Uehara H (2007) Polymer 48:7385
28. Kakiage M, Uehara H, Yamanobe T (2008) Macromol Rapid Commun 29:1571
29. Riekel C, Cedola A, Heidelbach F, Wagner K (1997) Macromolecules 30:1033
30. Uehara H, Yoshida R, Kakiage M, Yamanobe T, Komoto T (2006) Ind Eng Chem Res 45:7801
31. Capiati NJ, Porter RS (1975) J Mater Sci 10:1671. doi:10.1007/BF00554928
32. Cohen Y, Rein DM, Vaykhansky LE, Porter RS (1999) Compos Part A Appl Sci Manuf 30:19
33. Matabola KP, De Vries AR, Moolman FS, Luyt AS (2009) J Mater Sci 44:6213. doi:10.1007/s10853-009-3792-1
34. Hine PJ, Ward IM, Olley RH, Bassett DC (1993) J Mater Sci 28:316. doi:10.1007/BF00357801
35. Morye SS, Hine PJ, Duckett RA, Carr DJ, Ward IM (1999) Compos Part A Appl Sci Manuf 30:649